frontiers in Energy Research

ORIGINAL RESEARCH
published: 23 July 2021
doi: 10.3389/fenrg.2021.696608

Giga-Cycle Fatigue Behavior of the Nuclear Structure of 316L Weldments

Zhihong Xiong, Engao Peng, Lianghua Zeng and Qirong Xu*

School of Industrial Automation, Beijing Institute of Technology, Zhuhai, China

Some components made of 316L stainless steel in nuclear reactors are connected by welding, and these are under giga-cycle fatigue loading. Therefore, the giga-cycle fatigue behavior of 316L weldments, which are fabricated by Laser Beam Welding (LBW) and Gas Tungsten Arc Welding (GTAW), were investigated using an ultrasonic fatigue testing system. The results indicate that the fatigue strength of LBW-made weldments is almost the same as that of GTAW-made weldments even though the microstructure and mechanical properties of the weldments are different. For the LBW-made specimens, the LBW-induced internal pores with a diameter range of about 89–270 μm were observed in the fracture surface. However, an obvious decrease in fatigue life was not observed in such cases. For the GTAW-made specimens, the quality requirement of the weld seam has to be more strict to prevent fatigue strength from decreasing. The fatigue failure mode of the GTAW-made specimens is the same as that of LBW-made specimens in the high-cycle fatigue regime but different in the giga-cycle fatigue regime.

Keywords: nuclear reactor, giga-cycle fatigue, crack initiation, 316L, weldment

OPEN ACCESS

Edited by:
Zhang Chunyu,
Sun Yat-Sen University, China

Reviewed by:
Jinfeng Li,
Imperial College London, United Kingdom
Sam Manuel,
Oak Ridge National Laboratory, United States

****Correspondence:***
Lianghua Zeng
zhuhai09@sina.com

Specialty section:
This article was submitted to Nuclear Energy, a section of the journal Frontiers in Energy Research

Received: *17 April 2021*
Accepted: *01 June 2021*
Published: *23 July 2021*

Citation:
Xiong Z, Peng E, Zeng L and Xu Q (2021) Giga-Cycle Fatigue Behavior of the Nuclear Structure of 316L Weldments. Front. Energy Res. 9:696608. doi: 10.3389/fenrg.2021.696608

INTRODUCTION

Due to its excellent corrosive resistance, irradiation resistance, and mechanical properties, 316L austenitic stainless steel (316L) is widely used in the fabrication of nuclear components, which are usually connected by welding. These components usually suffer from giga-cycle loading during their service life, which can lead to catastrophic nuclear accidents after a certain period of time (Naoe et al., 2015; Han et al., 2016). Therefore, the knowledge of the fatigue properties of these weldings is very important to the design of components in the nuclear industry. The study of giga-cycle fatigue behavior of the 316L weldments is then necessary for the operation and lifetime management of the nuclear plants.

It has been reported that the fatigue behavior in the giga-cycle regime is different from that in the high-cycle fatigue regime (Ping et al., 2015; Su et al., 2017). In the giga-cycle fatigue regime, the conventional fatigue limit disappeared and the fatigue cracks initiate from the internal defect (such as pores, inclusions, and so on) due to the localized stress or strain concentration. A typical feature of giga-cycle fatigue, that is the so-called fish-eye, can be observed on the fracture surface. It is proposed that the characteristics of weld microstructures have a significant influence on the fatigue behavior of weldments (Ko, 1989; Yoshihisa and Raman, 2000; Iwata et al., 2006; Basu et al., 2013). The fatigue cracks usually initiate from subsurface or internal detects caused by welding in the giga-cycle fatigue regime. The reduction in the fatigue strength is caused by the existence of welding defects and a soft zone along with the welds (Deng et al., 2016; Hong and Sun, 2017; Zhang et al., 2018).

So far, there are many kinds of commercial welding methods, such as Laser Beam Welding (LBW), Gas Tungsten Arc Welding (GTAW), Submerged-Arc Welding, and so on. In general,

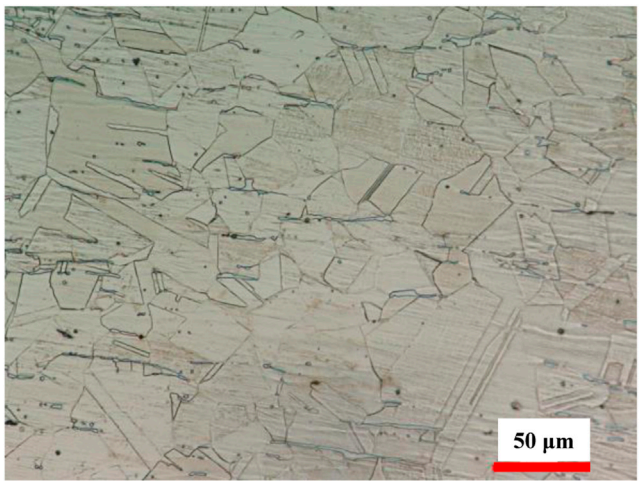

FIGURE 1 | Optical microstructure of the base metal.

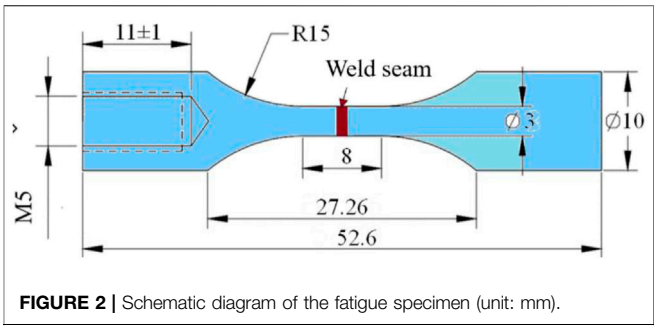

FIGURE 2 | Schematic diagram of the fatigue specimen (unit: mm).

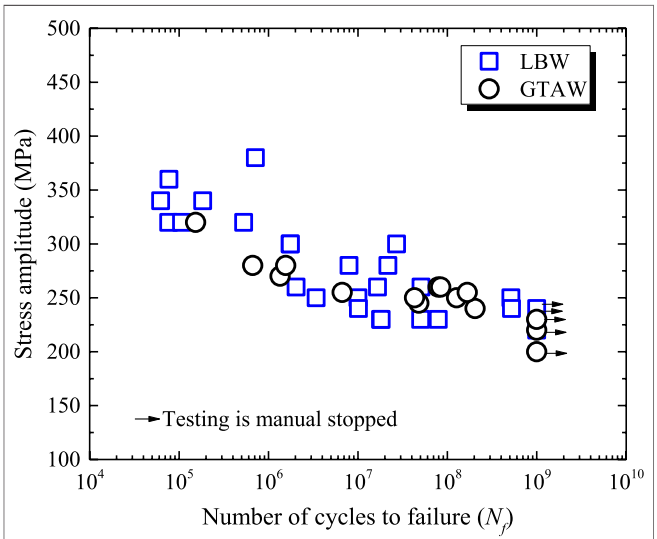

FIGURE 3 | Fatigue strength of the weldments made by BLW and GTAW.

the microstructure and mechanical properties of the weld seam are closely related to welding methods. For example, in the case of LBW, it is difficult to completely eradicate the pore due to the metal evaporation caused by the high energy density and protection gas captured by high cooling rate (Errico et al., 2020). And the fine grains are usually formed in the weld seam, leading to high hardness (Xiong et al., 2019a), which is different from the much lower hardness distributed in the weld seam induced by the much coarse grains in the case of GTAW (Xiong et al., 2019b). The size of the heat-affected zone of LBW-made weldment is also relatively smaller than that of GTAW-made weldment (Lee et al., 2014).

Although some investigations on the giga-cycle fatigue behavior of 316L base metal and weldment have been done (Carstensen et al., 2002; Naoe et al., 2015, 2018; Xiong et al., 2019b), the fatigue data of 316L, especially of the 316L weldment, is still insufficient. Besides, there have been very few studies thus far pertaining to how the welding method affects the giga-cycle fatigue behavior of 316L.

Therefore, to clarify the effects of the weld method on the fatigue behavior of the weldments, the giga-cycle fatigue behaviors of 316L weldments fabricated by LBW and by GTAW respectively were investigated by an ultrasonic fatigue-testing machine in this research. Thereafter, the fatigue strength and crack initiation mechanisms of the LBW-made weldments and the GTAW-made weldments are compared with each other. The fatigue fracture surface was investigated through Scanning Electron Microscopy (SEM) to clarify the fatigue crack initiation mechanism.

EXPERIMENT PROCEDURE

Materials and Specimens

In this study, 316L austenitic stainless steel (or ASTM A240, with the yield strength, ultimate tensile strength, and Vickers hardness of 319 MPa, 614 MPa, and 183, respectively) was selected as the base metal, and its representative austenitic microstructure is shown in **Figure 1**.

The details of LBW and GTAW can be referred to in our previous report (Xiong et al., 2019a; Xiong et al., 2019b). The specimens used for the fatigue test were machined following the geometry shown in **Figure 2**. Before fatigue testing, each specimen surface was polished along the axial direction using the 1,200# abrasive paper.

Ultrasonic Fatigue Test

The ultrasonic fatigue tests were conducted at Northwestern Polytechnical University (Xian, China) with a stress ratio of −1 at the frequency of 20 kHz. The test was manually stopped when the number of the fatigue cycles reached up to 10^9. In order to prevent the increase in the specimen temperature due to the high strain rate deformation, not only a periodic loading/resting interval was applied during the ultrasonic fatigue test, but also blasts of cold air were blown to the specimen surface. More details about the ultrasonic fatigue test can be found in the literature (Stanzl-Tschegg, 2014). The

TABLE 1 | Maximum diameter of the internal pore for the LBW-made weldments.

Stress amplitude (MPa)	Number of cycles to failure	Maximum diameter of the internal pore (μm)
230	1.82×10^7	111.1
230	7.93×10^7	166.1
240	1.01×10^7	123
240	5.22×10^8	246.4
250	1.00×10^7	150.6
260	5.08×10^7	178.6
280	2.16×10^7	271.7
300	2.71×10^7	89.3

fracture surfaces of the fatigued specimens were characterized by using SEM to reveal the fatigue crack initiation and propagation mechanism.

RESULTS AND DISCUSSION

Fatigue Strength of the Weldments Made by LBW and GTAW

The results of fatigue strength measurements for the weldments made by LBW and GTAW are presented in **Figure 3**.

It indicates that fatigue failure occurs in the very high cycle fatigue regime and the fatigue strength of the LBW-made weldment are almost the same as those of the GTAW-made weldment, although the microstructure and the properties of the weld seam are different, as reported in the author's previous studies (Xiong et al., 2019a; Xiong et al., 2019b).

In the case of GTAW, both base metal and weld seam exhibit typical austenitic equiaxed grains with a similar average grain size of about 40 μm and a similar hardness. No distinct welding defect is observed.

In the case of LBW, a fine dendrite structure is preferably formed at the center of the weld seam, resulting in the highest hardness. Conversely, coarse columnar crystals can be found at the edge of the weld line, resulting in lower hardness. Besides, some pores are observed in the weld seam. **Table 1** shows the diameter of the internal pore for the LBW-made weldments. It indicates that the maximum diameter of the internal pores caused by laser welding is in the range of about 89–270 μm. However, a clear decrease in fatigue life was not observed in such cases. That is, the fatigue life of the LBW-made weldment with internal pore, whose diameter is smaller than 270 μm, is not diminished compared to that of GTAW-weldments.

H.N. Ko shows that the fatigue strength increases as the grain size decreases (Ko, 1989). Besides, the fatigue strength can be roughly evaluated by tensile strength and hardness. The higher the tensile strength and hardness, the higher the fatigue strength is (Casagrande et al., 2011). Furthermore, the fatigue strength of the weldments is weakened due to the existing welding defects (Yoshihisa and Raman, 2000; Iwata et al., 2006).

Therefore, to clarify the effects of the welding process on the fatigue strength of the weldments, there are two kinds of influence factors that have to be considered: one is the property of the weld seam, such as grain size, morphology, and hardness, and the other is the welding defects, such as pores and poor fusion.

For the GTAW-made weldments, there is no pronounced difference in microstructure and hardness between weld seam and base metal, therefore, the welding process maybe has no clear side effect on fatigue strength. It can be deduced that the fatigue strength should be weakened if there were welding defects in the weld seam.

For the LBW-made weldments, the localized temperature is very high due to the high energy density of the heat source, leading to metal evaporation. Meanwhile, the cooling rate of the fusion metal is extremely high so that the protection gas cannot escape and is captured by the melted metal during solidification. Thus, it is difficult to completely eradicate the pore formed during laser welding. It is revealed that the existing welding flaws or inclusions are the favorite sites for crack initiation, and most of the fatigue failure occurs in the welding part, resulting in the decrease in the fatigue strength (Yoshihisa and Raman, 2000; Chandra et al., 2013; Stanzl-Tschegg, 2014). Hence, the welding defects existing in the weld are likely to do harm to the fatigue strength. On the other hand, refined crystalline strengthening, which is caused by the extremely high cooling rate, can enhance the fatigue strength of the weld seam. This means the existence of fine grains along the weld seam may compensate for the harmful effects of the existence of some welding defects at a certain size near the weld seam made by LBW, without decreasing the fatigue strength.

It is well-known that the main pipe connected by GTAW of primary circuit in the nuclear power plant is the channel to maintain and restrict the coolant circulation flow. It is closed with high temperature, high pressure, and radioactive coolant, which plays an important role in ensuring the safety and normal operation of the reactor. These components usually suffer from cyclic loading due to flow-induced vibrations, internal pressure, and thermal stress caused by temperature change during the service life of the reactors. Therefore, the service life of the reactor strongly depends on the fatigue life of the weldment, and the fatigue life of the weldment depends on the welding process and quality. According to the above discussions, to prevent the decrease in the fatigue strength of the weldments, the quality requirement for the weld seam made by GTAW has to be more strict than that for the LBW-made weld seam. In other words, the fatigue life of the GTAW-made weldment is more sensitive to internal defects caused by welding than that of the LBW-made weldment. For example, if both GTAW- and LBW-made weldments contain internal pores with a diameter of 100 μm, the fatigue life of GTAW-made weldments might decrease notably, but that of LBW-made weldment would not. Comparing to GTAW-made weldment, the safety factor of LBW-made weldment is higher. That is, from the viewpoint of fatigue strength, laser welding seems to be a potential alternative to replace GTAW used in nuclear reactor design and construction.

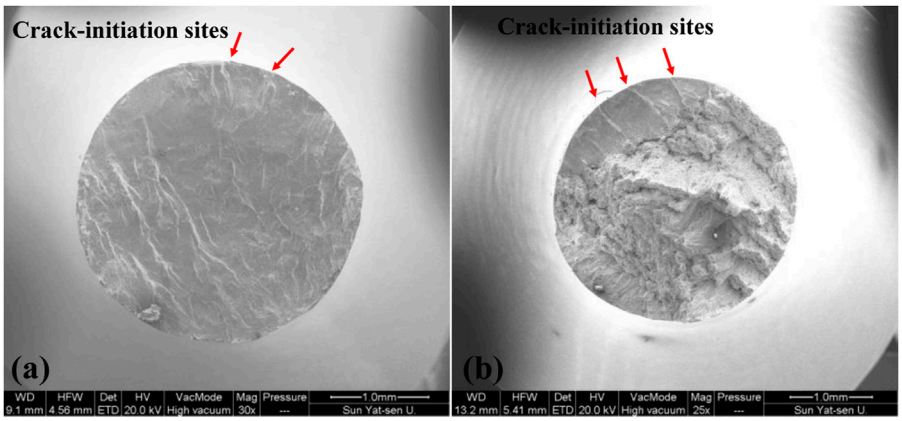

FIGURE 4 | Fracture surface of the specimens (GTAW) **(A)** failed under 320 MPa at 1.53×10^5 cycles (Xiong et al., 2019b) **(B)** failed under 250 MPa at 4.3×10^7 cycles.

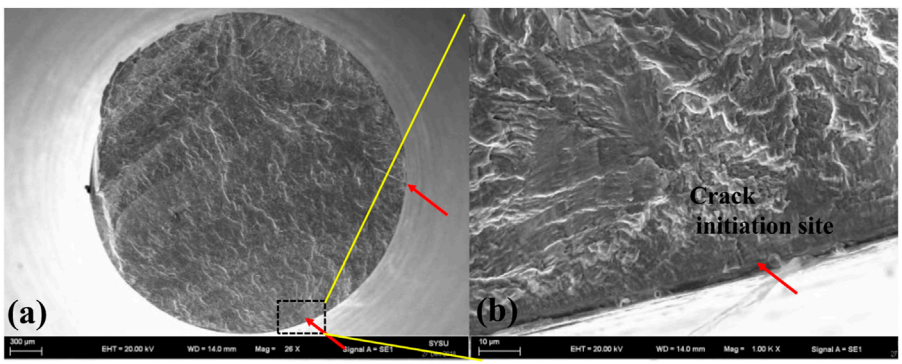

FIGURE 5 | Fracture surface of the specimen (LBW) tested at 340 MPa failed at 1.84×10^5 cycles. **(A)** overview of the fracture surface and **(B)** enlargement of the marked rectangle in **(A)**.

Crack Initiation and Propagation Mechanism

All of the fracture surfaces of the fatigue-tested specimens were examined by SEM. There are two fracture modes. One is that the fatigue cracks are initiated from the specimen surface due to crystal slip. The other one is that the fatigue cracks are initiated due to internal defects.

For the weldments made by GTAW, as reported in the previous paper (Xiong et al., 2019b), all of the specimens failed due to the surface crack initiation; no matter what kind of fatigue regime they are in, high-cycle fatigue regime or giga-cycle fatigue regime and multiple crack initiation sites can be recognized. **Figure 4** presents the typical surface crack initiation failure modes in the high- and giga-cycle fatigue regimes, respectively. As shown in **Figure 4B**, fatigue cracks initiate at the surface and then propagate inward, resulting in the formation of a smooth semi-elliptical area.

For the high-cycle fatigue test of weldments made by LBW, the fatigue failure is mostly caused by the surface crack initiation with multiple crack initiation sites (a typical fracture surface of the specimen is shown in **Figure 5**. This is similar to the failure mode of the specimens made by GTAW. In addition, the failure of several specimens is caused by the internal pores that are formed during laser welding, as shown in **Figure 6**.

In the giga-cycle fatigue regime, the fatigue failure mode of LBW sample is different from that in the high-cycle fatigue regime and the specimens made by GTAW. Most of the fatigue failure occurred is due to the internal or subsurface crack initiation. A typical internal crack initiation failure mode, for the specimen tested at 260 MPa failed at 5.08×10^7 cycles, is presented in **Figure 7**.

A very famous phenomenon for the internal defects causing giga-cycle fatigue failure, i.e., fish-eye, is observed in the crack initiation and propagation area, as shown in **Figure 7A**, and a clearer appearance is presented in **Figure 7B**. As shown in **Figure 7C**, at the center of the fish-eye is the origin of a fatigue crack, i.e., a pore introduced by LBW. After the crack initiation, it propagates along the direction perpendicular to the tangential of the circumference of the pore, and then a

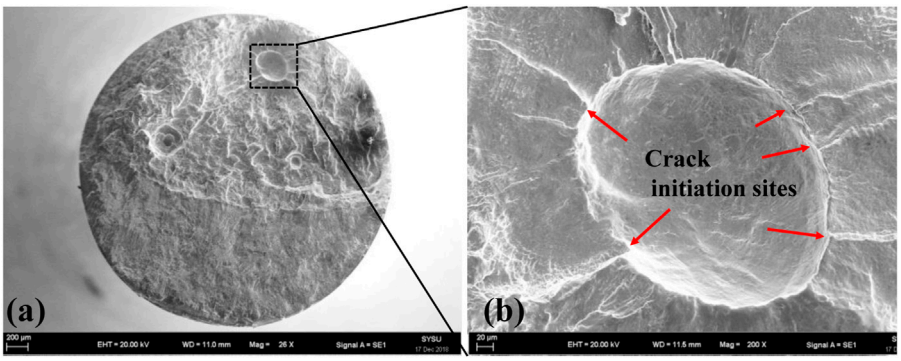

FIGURE 6 | Fracture surface of the specimen (LBW) tested at 380 MPa failed at 7.15×10^5 cycles. **(A)** overview of the fracture surface and **(B)** enlargement of the marked rectangle in **(A)**.

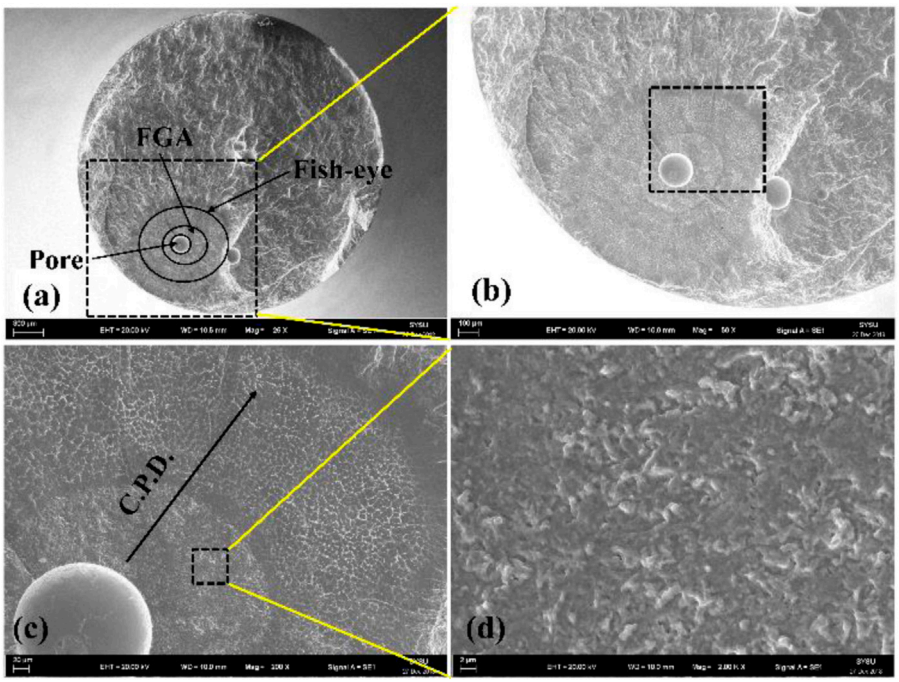

FIGURE 7 | Fracture surface of the specimen (LBW) tested at 260 MPa failed at 5.08×10^7 cycles. **(A)** overview of the fracture surface, **(B)** enlargement of the marked rectangle in **(A,C)** enlargement of the marked rectangle in **(B,D)** enlargement of the marked rectangle in **(C)**.

rough area called fine-granular area [FGA, see **Figure 7D**] is formed around the pore. Furthermore, outside of the FGA is a bright and relatively flat area, which is related to a different crack propagation rate.

In general, the fatigue cracks can initiate from both the specimen surface and the interior, which is the result of the competition between the stress concentration caused by surface defects and that caused by interior defects. When the concentrated stress caused by internal defects is higher enough, the fatigue crack would initiate from the interior. Otherwise, it initiates from the surface (Xin, 2010).

It has been proved that fatigue cracks prefer nucleating and propagating on specimen surfaces due to their geometric-mechanical conditions compared to the interior region. The fatigue failure is usually caused by the gradual growth of microcracks originated from slip bands formed on the specimen surface (Forsyth, 1957; Suresh, 1998). Therefore, when the specimen is under a high-stress amplitude, which is higher than the threshold value for persistent slip band (PSB) formation, i.e., in the high-cycle fatigue regime, the fatigue cracks usually originate from the specimen surface, as presented in **Figure 4** and **Figure 5**. However, if the stress caused by

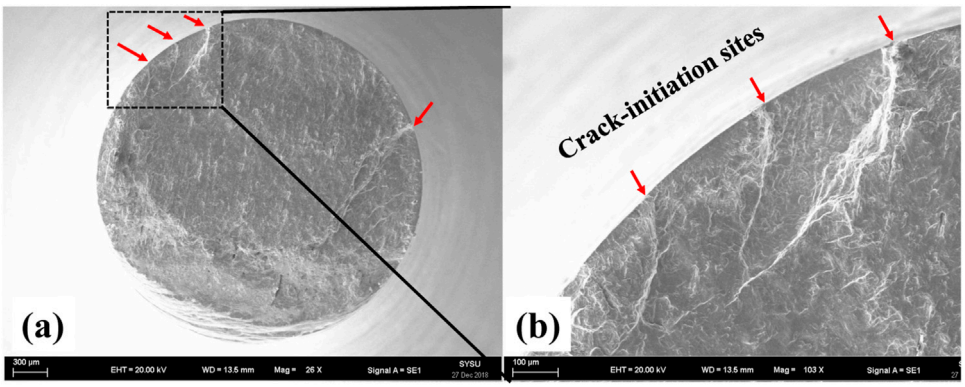

FIGURE 8 | Fracture surface of the specimen (LBW) tested at 250 MPa failed at 5.14×10^8 cycles. **(A)** overview of the fracture surface, **(B)** enlargement of the marked rectangle in **(A)**.

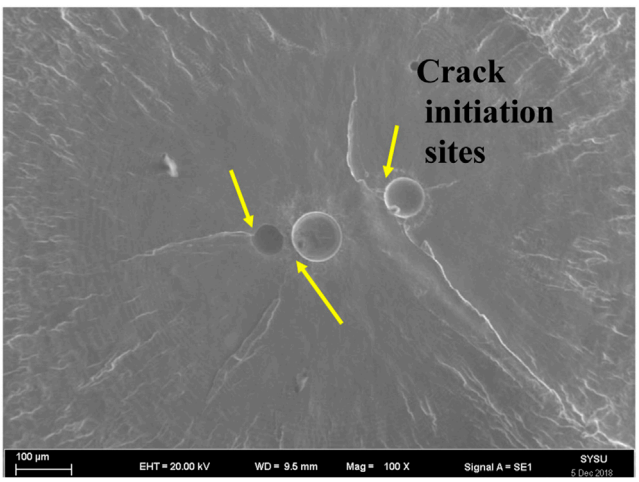

FIGURE 9 | The origins of a typical multiple cracks for the specimen (LBW) failed at 1.82×10^7 cycles.

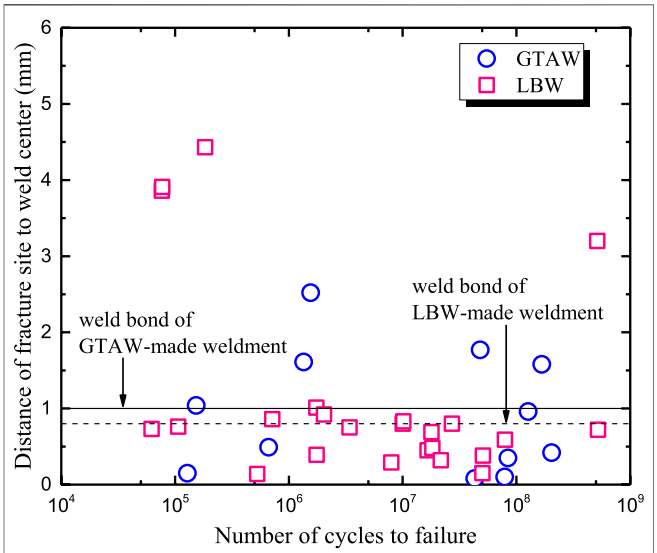

FIGURE 10 | Relationship fracture site and the number of cycles to failure.

interior defects is high enough, as shown in **Figure 6**, the fatigue cracks can also initiate from the interior pores.

It has been reported that, in the giga-cycle fatigue regime, the fatigue crack initiation mechanism is different from that in the high-cycle fatigue regime. The fatigue cracks in the high-cycle fatigue regime usually initiate from internal defects or inclusions for many kinds of materials, such as high-strength steel and various alloys (Li, 2012; Krewerth et al., 2013; Bathias and Wang, 2014; Grigorescu et al., 2016; Hong et al., 2016). Similar to that, in this research, most of the fatigue cracks also originate from the internal defects induced by LBW; only one fatigue failure occurred due to the surface crack initiation (as shown in **Figure 8**). This is similar to the failure mode of the specimens made by GTAW.

As proposed by Mughrabi (Mughrabi, 1999), for the materials without internal inclusions or with small inclusions, the fatigue cracks also can initiate from specimen surface due to the accumulation of slightly irreversible random slip on the surface defects, even the stress level is lower than the threshold value for PSB formation (i.e. in the giga-cycle fatigue regime). Therefore, in the case of specimens made by GTAW, there are no obvious welding defects in the weld seam due to the well-controlled weld quality. All of the specimens fail due to the accumulation of slightly irreversible random slip on the surface defects in the giga-cycle fatigue regime. This is different from the case of the LBW-made specimen.

Furthermore, Ma et al. (Ma et al., 2010) found most of the fatigue failures were caused by multiple-crack origins in high-cycle fatigue regimes while by single crack origin in giga-cycle fatigue regimes. The number of cracks origins decreases with the increase in fatigue life. Because most of the fatigue failure is related to the PSB formation in the high-cycle fatigue regime

(high stress level), the octahedral slip systems can be activated in more than one surface grain at different locations in the case of localized high stress, leading to multiple crack origins (Suresh, 1998; Chaussumier et al., 2010). However, as shown in **Figure 9**, the multiple crack origins for some LBW-made specimens are also observed in the giga-cycle fatigue regime, resulting from the stress or strain concentration caused by the LBW-induced pore cluster.

Fracture Site

Figure 10 shows the relationship between the distance of fracture site to weld center and the number of cycles to failure. The distance of fracture site to weld center is measured through careful observation of the fracture surface. The weld bonds of the GTAW-made and LBW-made weldment are represented by a solid line and dash line, respectively. For GTAW-made specimens, the fatigue failure occurs at base metal (BM) if the distance value is larger than 1 mm, otherwise, the specimen failed at weld metal (WM). For LBW-made specimens, the distance to distinguish BM and WM is 0.8 mm. It should be noted that the width of the weld seam for GTAW-made and LBW-made specimens are 2 and 1.6 mm, respectively.

It can be seen that the fracture location differs between the fatigued GTAW-made and LBW-made specimens. For the GTAW-made specimen, the fatigue fracture site is independent of the number of cycles to failure. Some of the specimens fail at the BM, and some of them fail at WM. That is, the fracture sites are distributed randomly. For the LBW-made specimen, it seems that the fracture site is related to the number of cycles to failure. The fracture sites are distributed randomly in the high cycle fatigue regime. This is similar to the case of the GTAW-made specimen. However, in the giga-cycle fatigue regime, most of the specimens fail at WM except one specimen.

As discussed in the previous section, for the GTAW-made specimen, all of the specimens failed due to the surface crack initiation, regardless of the number of cycles to failure. As the well-controlled welding process, there is no obvious welding defect at the weld seam. Besides, the BM and WM should have the same surface condition. This indicates they should have equal potential for fatigue failure. Therefore, fatigue crack randomly initiates at BM and WM, i.e., the fracture sites are randomly distributed. For the LBW-made specimen, similarly, the fracture site distributes randomly in the high-cycle fatigue regime. In the giga-cycle fatigue regime, fatigue crack usually originates from the internal pores caused by welding, i.e., the specimen fracture at WM. In a word, the transition of fracture site for the LBW-made specimen among different parts of the welds is related to the transition of fatigue failure mode.

CONCLUSION AND PROSPECT

In this research, the giga-cycle fatigue behavior of the 316L weldment fabricated by GTAW and by LBW has been investigated by using the ultrasonic fatigue testing system. The following conclusions have been drawn.

Firstly, the fatigue strength of weldments made by LBW is almost the same as that of weldments made by GTAW, although the microstructure and properties of the weldments were different. For the LBW-made specimen, it allows the existence of some welding defects at a certain size (less than 270 μm) in weld seam made by LBW, without decreasing the fatigue strength. For the GTAW-made specimens, the quality requirement of the weld seam has to be more strict than that by LBW to prevent the decrease in the fatigue strength.

Secondly, in the high cycle fatigue regime, the fatigue failure mode of the GTAW-made specimens is the same as that of LBW-made specimens, i.e., most of the specimens failed due to the surface crack initiation. In the giga-cycle fatigue regime, all of the specimens prepared using GTAW are failed due to the surface crack initiation, while internal defects are the primary reason to induce the failure of LBW-made samples.

In a word, LBW has some advantages in terms of fatigue resistance compared with GTAW. LBW seems to be a potential alternative process to replace GTAW used in the nuclear reactor design and construction. However, the service environment of the reactor components is very complex. Besides the fatigue resistance of the weldment, many other properties (corrosion resistance, irradiation resistance, and stress-corrosion resistance amongst other things) have to be considered and investigated during reactor design and construction.

Furthermore, pore clusters were observed in the fracture surface, which might have an influence on the giga-cycle fatigue behavior. Therefore, further investigation on the effect of pore cluster characteristics (the maximum size, distribution, number of pores, and so on) on fatigue behavior has to be conducted.

DATA AVAILABILITY STATEMENT

The raw data supporting the conclusion of this article will be made available by the authors, without undue reservation.

AUTHOR CONTRIBUTIONS

ZX carried out the experimental works, analysis and writing. LZ carried of the analysis of the microstructure and hardness of the weldment. QX carried out the analysis of the fatigue fracture surface. EP carried out some experiments.

FUNDING

This research was funded the Natural science foundation of the Guangdong province, Grant no. 2018A030310102.

REFERENCES

Basu, K., Das, M., Bhattacharjee, D., and Chakraborti, P. C. (2013). Effect of Grain Size on Austenite Stability and Room Temperature Low Cycle Fatigue Behaviour of Solution Annealed AISI 316LN Austenitic Stainless Steel. *Mater. Sci. Technol.* 23, 1278–1284. doi:10.1179/174328407X179575

Bathias, C., and Wang, C. (2014). Initiation from Low Cycle Fatigue to Gigacycle Fatigue. *AMR* 891-892, 1419–1423. doi:10.4028/www.scientific.net/amr.891-892.1419

Carstensen, J. V., Mayer, H., and Brøndsted, P. (2002). Very High Cycle Regime Fatigue of Thin Walled Tubes Made from Austenitic Stainless Steel. *Fatigue Fract Eng. M* 25, 837–844. doi:10.1046/j.1460-2695.2002.00554.x

Casagrande, A., Cammarota, G. P., and Micele, L. (2011). Relationship between Fatigue Limit and Vickers Hardness in Steels. *Mater. Sci. Eng. A* 528, 3468–3473. doi:10.1016/j.msea.2011.01.040

Chandra, S. K., Shankar, V., Mariappan, K., Sandhya, R., and Chakraborty, P. C. (2013). Effect of Strain Rate on the Low Cycle Fatigue Behavior of 316L(N) Stainless Steel Weld Joints. *Proced. Eng.* 55, 176–180. doi:10.1016/j.proeng.2013.03.239

Chaussumier, M., Shahzad, M., Mabru, C., Chieragatti, R., and Rezaï-Aria, F. (2010). A Fatigue Multi-Site Cracks Model Using Coalescence, Short and Long Crack Growth Laws, for Anodized Aluminum Alloys. *Proced. Eng.* 2, 995–1004. doi:10.1016/j.proeng.2010.03.108

Deng, C., Wang, H., Gong, B., Li, X., and Lei, Z. (2016). Effects of Microstructural Heterogeneity on Very High Cycle Fatigue Properties of 7050-T7451 Aluminum alloy Friction Stir Butt Welds. *Int. J. Fatigue* 83, 100–108. doi:10.1016/j.ijfatigue.2015.10.001

Errico, V., Campanelli, S. L., Angelastro, A., Mazzarisi, M., and Casalino, G. (2020). On the Feasibility of AISI 304 Stainless Steel Laser Welding with Metal Powder. *J. Manufacturing Process.* 56, 96–105. doi:10.1016/j.jmapro.2020.04.065

Forsyth, T. (1957). Thomas Forsyth to Lewis Cass, St. Louis October 24, 1831: Draper Mss. 6T152-164. *Ethnohistory* 4, 198–202. doi:10.2307/480716

Grigorescu, A. C., Hilgendorff, P.-M., Zimmermann, M., Fritzen, C.-P., and Christ, H.-J. (2016). Cyclic Deformation Behavior of Austenitic Cr-Ni-Steels in the VHCF Regime: Part I - Experimental Study. *Int. J. Fatigue* 93, 250–260. doi:10.1016/j.ijfatigue.2016.05.005

Han, Y., Mei, J., Peng, Q., Han, E.-H., and Ke, W. (2016). Effect of Electropolishing on Corrosion of Nuclear Grade 316L Stainless Steel in Deaerated High Temperature Water. *Corrosion Sci.* 112, 625–634. doi:10.1016/j.corsci.2016.09.002

Hong, Y., Liu, X., Lei, Z., and Sun, C. (2016). The Formation Mechanism of Characteristic Region at Crack Initiation for Very-High-Cycle Fatigue of High-Strength Steels. *Int. J. Fatigue* 89, 108–118. doi:10.1016/j.ijfatigue.2015.11.029

Hong, Y., and Sun, C. (2017). The Nature and the Mechanism of Crack Initiation and Early Growth for Very-High-Cycle Fatigue of Metallic Materials - an Overview. *Theor. Appl. Fracture Mech.* 92, 331–350. doi:10.1016/j.tafmec.2017.05.002

Iwata, T., Matsuoka, K., and Kobayashi, Y. (2006). Fatigue Strength of Welded Joints of SUS316L for Chemical Tankers. *Weld World* 50, 82–91. doi:10.1007/BF03263448

Ko, H. N. (1989). Effect of Grain Size on Fatigue Strength of Sintered Al2O3 under Rotary Bending. *J. Mater. Sci. Lett.* 8, 1438–1441. doi:10.1007/BF00720216

Krewerth, D., Weidner, A., and Biermann, H. (2013). Application of *In Situ* Thermography for Evaluating the High-Cycle and Very High-Cycle Fatigue Behaviour of Cast Aluminium alloy AlSi7Mg (T6). *Ultrasonics* 53, 1441–1449. doi:10.1016/j.ultras.2013.03.001

Lee, J. H., Park, S. H., Kwon, H. S., Kim, G. S., and Lee, C. S. (2014). Laser, Tungsten Inert Gas, and Metal Active Gas Welding of Dp780 Steel: Comparison of Hardness, Tensile Properties and Fatigue Resistance. *Mater. Des.* 64 (dec), 559–565. doi:10.1016/j.matdes.2014.07.065

Li, S. X. (2012). Effects of Inclusions on Very High Cycle Fatigue Properties of High Strength Steels. *Int. Mater. Rev.* 57, 92–114. doi:10.1179/1743280411Y.0000000008

Ma, X.-F., Duan, Z., Shi, H.-J., Murai, R., and Yanagisawa, E. (2010). Fatigue and Fracture Behavior of Nickel-Based Superalloy Inconel 718 up to the Very High Cycle Regime. *J. Zhejiang Univ. Sci. A.* 11, 727–737. doi:10.1631/jzus.a1000171

Mughrabi, H. (1999). On the Life-Controlling Microstructural Fatigue Mechanisms in Ductile Metals and Alloys in the Gigacycle Regime. *Fatigue Fracture Eng. Mater. Structures* 22, 633–641. doi:10.1046/j.1460-2695.1999.00186.x

Naoe, T., Xiong, Z., and Futakawa, M. (2016). Gigacycle Fatigue Behaviour of Austenitic Stainless Steels Used for Mercury Target Vessels. *J. Nucl. Mater.* 468, 331–338. doi:10.1016/j.jnucmat.2015.07.040

Naoe, T., Xiong, Z., and Futakawa, M. (2018). Temperature Measurement for *In-Situ* Crack Monitoring under High-Frequency Loading. *J. Nucl. Mater.* 506, 12–18. doi:10.1016/j.jnucmat.2017.12.019

Ping, Z., Gao, G., Misra, R. D. K., and Bai, B. (2015). Effect of Microstructure on the Very High Cycle Fatigue Behavior of a Bainite/martensite Multiphase Steel. *MATER. SCI. ENG. A.* 630, 1–7. doi:10.1016/j.msea.2015.02.015

Stanzl-Tschegg, S. (2014). Very High Cycle Fatigue Measuring Techniques. *Int. J. Fatigue* 60, 2–17. doi:10.1016/j.ijfatigue.2012.11.016

Su, H., Liu, X., Sun, C., and Hong, Y. (2017). Nanograin Layer Formation at Crack Initiation Region for Very-High-Cycle Fatigue of a Ti-6Al-4V alloy. *Fatigue Fract Engng Mater. Struct.* 40, 979–993. doi:10.1111/ffe.12562

Suresh, S. (1998). *Fatigue of Materials*. Cambridge: Cambridge University Press. doi:10.1017/cbo9780511806575

Xin, L. S. (2010). *Very High Cycle Fatigue Properties of High Strength Steels: Effects of Nonmetallic Inclusions*. BeiJing: Metallurgical Industry Press.

Xiong, Z. H., Ma, X. F., and Qi, X. Y. (2019a). Very High Cycle Fatigue Behaviour of the 316L Weldment Fabricated by Laser Butt-Welding. *IOP Conf. Ser. Mater. Sci. Eng.* 538, 012025. doi:10.1088/1757-899X/538/1/012025

Xiong, Z., Wei, D., Wang, H., Shi, H.-J., and Ma, X. (2019b). Fatigue Behavior of 316 L Stainless Steel Weldment up to Very-High-Cycle Fatigue Regime. *Mater. Res. Express* 6, 076514. doi:10.1088/2053-1591/ab1197

Yoshihisa, E., and Ganesh Sundara Raman, S. (2000). Thermomechanical and Isothermal Fatigue Behaviour of Type 316 Stainless Steel Base Metal, weld Metal, and Joint. *Sci. Technol. Welding Joining* 5, 174–182. doi:10.1179/136217100101538173

Zhang, W. C., Zhu, M. L., Wang, K., and Xuan, F. Z. (2018). Failure Mechanisms and Design of Dissimilar Welds of 9%Cr and CrMoV Steels up to Very High Cycle Fatigue Regime. *Int. J. Fatigue*, 367–376. doi:10.1016/j.ijfatigue.2018.04.032

Conflict of Interest: The authors declare that the research was conducted in the absence of any commercial or financial relationships that could be construed as a potential conflict of interest.